

# Observations of boundary layer structure and dynamics over a coastal urban area during extreme heat events

Gabriel Rios <sup>1\*</sup>, <sup>2\*</sup>, Prathap Ramamurthy <sup>1, 2</sup>

1. Department of Mechanical Engineering, CUNY City College, New York, New York

2. NOAA Center for Earth System Sciences and Remote Sensing Technologies, New York, New York

**Corresponding author:** Gabriel Rios ([grios001@citymail.cuny.edu](mailto:grios001@citymail.cuny.edu))

**\* Current affiliation(s):** Department of Mechanical Engineering, CUNY City College, New York, New York; NOAA Center for Earth System Sciences and Remote Sensing Technologies, New York, New York

For submission to the International Journal of Climatology.

*Last updated:* March 31, 2022.

---

## Abstract

Extreme heat presents a significant risk to human health and infrastructure in cities. Several studies have been conducted in the past several decades to understand the interaction between the synoptic-scale extreme heat events and local-scale urban heat island effects. However, observations of boundary layer characteristics during these periods have been relatively rare, especially in the vertical direction. Our current understanding of urban boundary layer structure is incomplete, particularly in coastal environments where the local climatology is highly influenced by land-sea thermal gradients. In this study, we analyze the evolution and structure of the urban boundary layer during regular and extreme heat periods with the goal of better understanding the effect of extreme heat and sea breezes on the boundary layer over a coastal urban area. Our analysis focuses on the New York City metropolitan area and relies on observations from vertical profilers (Doppler lidar, microwave radiometer), satellite data, and quantities derived by analytical methods. Extreme heat events present a mean peak surface temperature increase of 7 K, an increase of site-averaged specific humidity at the surface by 39.4%, and a marked southwesterly shift in winds at all sites. Positive anomalies of potential temperature and specific humidity are most prominent near the surface during morning periods and in the afternoon mixed layer during extreme heat events ( $\leq 1\sigma$ ). In addition, sea breeze events during heat extreme heat events are found to reduce temperatures and increase low-level moisture content from the early evening through nighttime hours, with strong variability between sites. The study also finds that extreme heat events unify horizontal wind directions throughout the boundary layer, and promote nocturnal onshore moisture transport.

## 1 Introduction

Extreme heat poses a major risk to life and property. The effects of extreme heat are expected to impact cities especially, presenting a significant hazard for vulnerable populations and infrastructure. With regards to effects on public health, studies have shown that extreme and prolonged heat increases mortality and exacerbates existing health conditions in high-risk populations (Anderson and Bell, 2011; Frumkin, 2016; Heaviside et al., 2017; Madrigano et al., 2015). With regards to effects on infrastructure, studies have shown that extreme heat subjects networks critical to urban areas (e.g., electrical grid, public transportation) under significant stresses and/or failure (McEvoy et al., 2012; Zuo et al., 2015).

These events are projected to increase in frequency due to the effects of climate change. Projections indicate that the impacts of future climate will cause adverse effects of extreme heat on cities to become more frequent and severe (Burillo et al., 2019; Forzieri et al., 2018; Peng et al., 2011).

The meteorology of extreme heat events and its impacts on urban areas can be observed from the synoptic and local scales. From a synoptic scale, extreme heat events are often caused by the sustained presence of a high-pressure system over an area, resulting in lower horizontal wind speeds and warm air subsidence, promoting higher surface temperatures (Black et al., 2004; Miralles et al., 2014). From a local perspective, the amplified impact of extreme heat events on cities is a result of the urban heat island (UHI) effect, which occurs as a result of the modification of land surface properties due to the built environment; recent work has shown an agglomeration of hot spots in urban areas during extreme heat episodes (Shreevastava et al., 2021). The modification of surface properties has been shown to increase near-surface air temperatures due to factors such as radiation entrapment, increased heat storage, and lower evapotranspirative cooling (F. Chen et al., 2014; Li and Elie Bou-Zeid, 2013; Ramamurthy and Bou-Zeid, 2017; Zhao et al., 2018). Urban areas near large bodies of water also experience effects from the sea breeze, which has been shown to play a moderating influence on the intensity of the UHI effect (Hu and Xue, 2016; Jiang et al., 2019; Stéfanon et al., 2014). The processes on these two scales can be connected by understanding the structure and dynamics of the urban boundary layer (UBL), which is the lowest part of the troposphere in which surface-atmosphere exchanges occur that directly affect human activity.

There have been a large number of numerical studies performed to improve our understanding of UBL processes during extreme heat events, which have been important for conceptualizing the role of synoptic-scale and local forcings on urban climate. Numerical models also allow for the resolution of spatial gaps that exist in many observational networks, particularly those in areas with heterogeneous surface properties (such as urban areas). Among the numerous studies that accomplish this, many recent papers have focused on the UBL over New York City. Meir et al. (2013) and Thompson et al. (2007) used numerical models to investigate various facets of the urban heat island and its interaction with Atlantic sea breezes over New York City, which allowed for high-resolution simulations of conditions and dynamics in a coastal urban area with complex land cover properties. Moreover, Bauer (2020) investigated these factors in the vertical using the Weather Research and Forecasting (WRF) model, allowing for a general visualization of the effects of roughness elements (such as supertall skyscrapers) on UBL dynamics. Ramamurthy and Bou-Zeid (2017) used a sophisticated urban canopy model as an addition to the WRF model to improve model representations of energy transfer into the UBL and its effects on the UHI effect, whereas Ortiz et al. (2018) also used the WRF model with an urban canopy parameterization and a building energy model to provide a more in-depth analysis of the UBL vertical structure during extreme heat events. However, critical details on the vertical structure and dynamics of the urban boundary layer have been missing in numerical experiments, such as the diurnal evolution of heat, moisture, and momentum throughout the mixed layer to the UBL height. One reason for this stems from the inability of current planetary boundary layer schemes to capture the complex land atmosphere interactions over large cities (González et al., 2021).

Despite the significant progress made in researching UBL phenomena at multiple scales, few observations of the UBL, particularly the mixed layer, exist in the literature. Observations of the UBL are critical for answering open questions in urban meteorology and for serving as input and validation datasets to high-resolution numerical weather models (Barlow, 2014; Best, 2005; Edwards et al., 2020; Leroyer et al., 2014; Ronda et al., 2017). These observations in the UBL have been limited, in part, due to the lack of availability of remote sensing instruments that can observe UBL properties with a sufficient spatiotemporal resolution (Barlow, 2014; Davis et al., 2021; Roth, 2000; Y. Zhang et al., 2020). Over the last 20 years, microwave radiometers, lidars, and radiosondes have been shown to be essential for accomplishing this. Microwave radiometers have been used to determine vertical profiles of temperature and water vapor

(Rose et al., 2005; Z. Wang et al., 2012), while lidars being used to observe three-dimensional wind fields and aerosol concentrations (Grund et al., 2001). Although radiosondes provide direct measurements of the aforementioned properties in the boundary layer as it moves vertically through it, they present greater difficulties (e.g., cost, shorter supply) and are unable to observe at the temporal resolution of microwave radiometers and lidars.

Although somewhat limited in spatiotemporal scale, numerous observational campaigns have been performed to better our understanding of UBL structure and dynamics. Barlow et al. (2011) provides an in-depth study of boundary layer dynamics above London over a month-long period using a combination of a sonic anemometer and Doppler lidar, allowing for high-resolution vertical observations of a complex UBL and a better understanding of turbulent structures and vertical mixing processes. Similarly, Pelliccioni et al. (2012) employs a sonic anemometer and a sodar system at a site in Rome to observe and analyze the lower 200 m of the UBL to determine UBL characteristics and explore the validity of Monin-Obukhov similarity theory in the surface layer. Additionally, Arruda Moreira et al. (2020) evaluates the ability of lidar and microwave radiometer systems to observe turbulence over a variety of atmospheric conditions, including the effects of significant dust concentrations, in the region around Granada, Spain. Studies such as those performed by Banks et al. (2015), Quan et al. (2013), and Z. Wang et al. (2012) further demonstrate the ability of vertical profiling instruments to analyze the boundary layer structure by deriving UBL heights and its diurnal evolution. Expanding upon UBL structure, Anurose et al. (2018) details a long-term observational campaign over an urban location in southern India that chronicles UBL height through monsoon season, annual averages of near-surface quantities, and the dynamics and effects of the sea breeze circulation.

Observations of the UBL during extreme heat events are even more limited. Prathap Ramamurthy et al. (2017) used microwave radiometers to observe the UBL over New York City in July 2016 to find that the UHI effect was amplified during heat wave events and that spatial variability throughout the city was significant throughout the observation period. Jiang et al. (2019) explores the effects of heat waves on rural and urban areas for several cities in China using ground-based observations with a focus on the UHI effect, finding that the effect was amplified during heat waves due to greater surface solar radiation and shifts in wind direction contributing to advection of heated air masses over the studied cities. (Wu et al., 2019) uses a combination of a ceilometer and multiple lidars to observe the evolution of UBL structure, air quality, and pollutant transport during a heat wave in New York City, demonstrating sharp rates of UBL growth due to convective activity and an increase of pollutant concentration and regional transport. Y. Zhang et al. (2020) uses aircraft-based observations to provide a comprehensive analysis of UBL structure during heat wave events over cities in the United States throughout a 10-year period, providing insights into the 'heat dome' thermodynamic structure over cities and the variability between heat wave events due to local (such as surface properties in urban areas) and large-scale (such as synoptic meteorological conditions) forcings.

New York City represents a complex case for urban meteorology given its diverse array of land cover types (deciduous forest to supertall skyscrapers) and its proximity to multiple major bodies of water (Lower New York Bay and the New York Bight to the south and east, Long Island Sound to the north and east). Due to these factors, the effects of the surface energy budget (Hrisko et al., 2021; Prathap Ramamurthy and Bou-Zeid, 2014; Tewari et al., 2019) and sea breezes (Childs and Raman, 2005; Colle and Novak, 2010; Frizzola and Fisher, 1963; Gedzelman et al., 2003; Han et al., 2022; Melecio-Vázquez et al., 2018; Thompson et al., 2007) on the mesoscale meteorology have been studied extensively. However, similar to studies of other urban areas mentioned previously, much of this research has involved numerical simulations of these meteorological processes. In this study, we attempt to further our understanding of the UBL over a coastal urban area by compiling observations from multiple locations within New York City and analyzing the UBL using derived quantities.

This study attempts to use observations and analytical methods to provide insight into the following questions:

1. How do UBL structure and dynamics depart from the climatology during extreme heat events?
2. How do extreme heat events impact the transport of scalars?
3. What effect does the sea breeze have on a coastal urban area during extreme heat events?

This paper is organized as follows. Section 2 discusses the study area and the properties of the observation sites within it, the instruments used and their properties, as well as data statistics and quality filtering methods. Section 3 presents observed and derived findings of UBL scalar properties and structure (temperature, moisture) and UBL dynamics. Section 4 presents the effects of the sea breeze on New York City during normal days and days with extreme heat. The results presented in these sections are discussed, compared with findings from previous related studies, and summarized in Section 5.

## 2 Data collection and analysis

### 2.1 Study sites

The New York City metropolitan area consists of over 20 million people (Bureau, 2021) and extends from New Jersey to Connecticut, spanning a diverse array of land cover types and geographic features. The mesoscale meteorology of New York City is strongly influenced by its coastal location, which is comprised of coasts on the New York Bight and Long Island Sound, both of which are arms of the Atlantic Ocean. Proximity to the coast results in strong land-sea thermal gradients, producing a complex array of sea breeze fronts that have highly variable effects on the city (Bornstein and Thompson, 1981; Gedzelman et al., 2003). With regards to New York City proper, heavy urbanization has resulted in a majority of its land cover being composed of impervious artificial surfaces (e.g., asphalt, concrete), resulting in significant contributions to the local climate.

Observational data was collected at three locations within New York City. The observational sites used for this study are located in the boroughs of The Bronx, Queens, and Staten Island, as shown in Figure 1. Building heights from the New York Primary Land Use Tax Lot Output database were aggregated and area-averaged for building height estimates shown in Table 1. The Bronx is the northernmost borough of New York City and features a varying degree of urbanization, ranging from a mixture of medium- and high-rise residential buildings and industrial warehouses in the southeastern Bronx to low-density residential and open vegetated areas (e.g., Van Cortlandt Park) in the northern and western Bronx. The Bronx observation site is located on the campus of Lehman College, approximately 3 km east of the Hudson River, and is surrounded by medium- and high-density residential and commercial areas on 3 sides with a small reservoir (area of 0.42 km<sup>2</sup>) to the west. Queens is the easternmost borough of New York City and features high-density residential and commercial buildings in the western portion of the borough, medium- to high-rise residential building and industrial warehouses in the south, and low- to medium-density residential buildings and vegetated open spaces (e.g. Flushing Meadows Corona Park) in the central and eastern portions of the borough deeper into Long Island. The Queens observation site is located on the campus of Queens College, due east of Flushing Meadows Corona Park, and is surrounded by medium-density residential and commercial areas on 3 sides. Staten Island is the southernmost and westernmost borough of New York City, featuring significantly lower degrees of urbanization relative to the rest of New York City. Land use on Staten Island is predominantly low-density residential and commercial, with large open and forested spaces on the western portion (e.g., Freshkills Park) and central portion (Todt Hill Woodlands and Latourette Park). Additionally, Staten Island features more variable terrain relative to the rest of New York City, with modest hills reaching 125 m at the highest point of

the island. The Staten Island observation site is located on the campus of the College of Staten Island, which is surrounded by forested and low-density residential areas.

Table 1: Locations and details of observations sites.

	Bronx	Queens	Staten Island
Coordinates	40.8725°N, -73.8935°E	40.7343°N, -73.8159°E	40.6040°N, -74.1485°E
Elevation (m a.g.l.)	57.8	56.3	32.4
Area-avgd. building height (m a.g.l.)	9.23	6.22	5.24
Area-avgd. land cover type	NLCD Developed, high density	Developed, medium density	Developed, low density

## 2.2 Observational instruments

Observations of the UBL were made using a synthesis of microwave radiometers, lidars, and satellites.

Vertical profiles of temperature and vapor density were captured using a network of Radiometrics MP-3000A microwave radiometers (Hewison and Gaffard, 2003) operated by the New York State Mesonet (Brotzge et al., 2020). Profiles for water vapor are retrieved using 21 channels in the 22-30.0 GHz (K-band) range, while profiles for temperature are retrieved using 14 channels in the 51-59.0 GHz (V-band) range. Profile accuracy (relative to radiosonde soundings) determined by performance studies at various locations reported an annually-averaged water vapor accuracy within  $1.0 \text{ g m}^{-3}$  below 2 km and an annually-averaged temperature accuracy within 1.6 K below 4 km (Güldner and Spänkuch, 2001; Sánchez et al., 2013). Quantities are captured at 58 height levels starting at ground level and ending at 10 km above ground level, with vertical steps of 50 m from ground level to 500 m, 100 m from 500 m to 2 km, and 250 m steps above 2 km. Observation integration times range from 0.01 to 2.50 s. Vertical profiles are generated every 10 s and averaged over 10 min periods.

Wind measurements were measured using a network of Leosphere WindCube 100S Doppler lidars operated by the New York State Mesonet (Brotzge et al., 2020). Measurements of wind motion using the Doppler beam swinging scan mode in three directions: zonal ( $u$ ), meridional ( $v$ ), and vertical ( $w$ ) over 20 s cycles, with measurements averaged over 10 min intervals (Shrestha et al., 2021). The vertical range of the WindCube 100S is 7 km above ground level with wind speed and direction accuracies of  $0.5 \text{ m s}^{-1}$  and  $2^\circ$ , respectively. The WindCube 100S has also been shown to perform with a high degree of accuracy relative to radiosonde soundings, especially above 500 m (Kumer et al., 2014).

Land and sea surface temperatures were estimated using derived products from the NOAA/NASA GOES-16 Advanced Baseline Imager (ABI) (Ignatov et al., 2010; Y. Yu et al., 2008). The GOES-16 ABI provides a spatial resolution of 2 km with real-time data available to the public on an hourly basis. The spatial extent of the Land Surface Temperature (LST) product ranges from the continental United States (CONUS) to the majority of the Western Hemisphere (known as *full disk*), whereas the Sea Surface Temperature (SST) product has a full disk spatial extent. The LST product has been found to have an error relative to surface observations of 2.5 K over all land cover types, while sea surface temperatures (SSTs) estimated using the GOES-16 ABI have been found to have an error relative to shipborne radiometers  $\leq 1 \text{ K}$  in the New York Bight (Luo and Minnett, 2021).

### 2.2.1 Data criteria & availability

Dates selected for this study are categorized into three groups: (1) normal days, (2) extreme heat days, and (3) sea breeze days. For the purposes of this study, *extreme heat events* are defined as 3 or more consecutive days with maximum daily temperatures exceeding 90°F (305 K), per the New York branch

of NOAA National Weather Service (National Weather Service, 2018; Robinson, 2001), while *normal days* are defined as days that do not meet these criteria. Because the aim of this study is to observe the effect of extreme heat on the UBL, normal day selection was restricted to months in which extreme heat events occurred (May through September), as well as days in which 50% or more of the day featured clear-sky conditions below 3.65 km above ground level due to the association of extreme heat events with reduced daytime cloud coverage and precipitation (Stéfanon et al., 2014; Thomas et al., 2020). Clear-sky conditions were identified by using an average of 5-minute surface-based observations from three airports in the Automated Surface Observation System (ASOS) (NOAA et al., 1998) network within the New York City metropolitan area: Newark Liberty International Airport (EWR) (40.6895°N, -74.1745°E), John F. Kennedy International Airport (40.6413°N, -73.7781°E), and LaGuardia Airport (40.7769°N, -73.8740°E). *Sea breeze events* are identified as times during normal and extreme heat days in which the low-level ( $\leq 200$  m) mean horizontal wind speed ( $U$ ) is less than  $5 \text{ m s}^{-1}$  and low-level wind direction has a primarily easterly component, due to the presence of the New York Bight and Long Island Sound to the east of New York City.

Observations from 102 days classified as normal and 87 days classified as extreme heat days were used for this study. The observation period lasted from June 2018 to September 2021 and days were selected between the months of May and September, as described previously. Quality filtering was performed for microwave radiometer and lidar data. For microwave radiometer data, the retrieval of vertical profiles of brightness temperature (from which derived values, such as temperature and vapor density) are obtained continuously through 7 km above ground level with bi-weekly tip calibrations to reset the K-band (Shrestha et al., 2021). For lidar data, data with carrier-to-noise ratio (CNR) values below -27 dB were rejected (Kumer et al., 2014; Shrestha et al., 2021) due to poor retrieval quality.

Microwave radiometer observation counts ranged between 200 and 250 hourly observation counts per site per selected height, with increased availability due to the robustness of the sensing method. The lower observation count at Staten Island is due to intermittent hardware issues preventing observations or storage of observational data. Lidar data observation counts (normal and extreme heat) average between 100 and 200 for every hour at 100, 500, and 1000 m with lower counts at 2000 m due to poor data availability because of increased scattering and noise. At lower heights, wind directions influenced by local factors result in higher observation counts from most directions with the exception of true northerly winds. As observation height increases, synoptic-scale factors dominate the observation count, with most observed winds coming from the west or southwest. Visualizations of observational statistics can be seen in the Appendix.

Using data from microwave radiometer and lidar observations, several quantities were derived to better understand UBL behavior. These quantities include mixing ratio, specific humidity, potential temperature, and mixed layer height. The methodology for these derivations is provided in the 5.

### 3 Normal and extreme heat boundary layer properties

This section discusses the differences in boundary layer structure and properties between normal days and extreme heat events. Results are presented from the averages over all identified normal and heat event days.

#### 3.1 Temperature

On average, extreme heat events increase the temperature at the surface, as expected (see Figure 3). This is consistent across all observed locations in New York City, with the extreme heat event temperature exceeding normal temperatures by approximately  $1\text{-}\sigma$  over the entire day. An increase in



the difference is observed during daytime hours, with the difference peaking in magnitude around 13:00 LST at the hottest time of day. The surface temperature variability is significantly lower during heat events (average  $\sigma = 1.77$  K) than during normal temperatures (average  $\sigma = 4.57$  K). There is little spatial variability between sites, with maximum average temperatures ranging from 305.65 K in Queens to 306.63 K in the Bronx. It is worth noting that there are areas in New York City that are located in more heavily urbanized areas than the observation sites (such as Midtown Manhattan and central Brooklyn), so it is likely that certain areas within the city have higher maximum temperatures.

Above the surface, extreme heat events increase the temperature significantly over the lowest 3000 m of the troposphere (see Figure 2), with standardized anomalies of  $\theta$  ranging from  $\sigma = 0.99$  to 1.30. The largest temperature anomalies shift from the surface layer in the mornings to span the entirety of the mixed layer in the afternoon. This is reflective of strong surface forcing resulting in convection through the mixed layer, as indicated by the formation of a late morning superadiabatic layer at all locations (Figure 4).

The vertical profiles of  $\theta$  suggest a degree of spatial variability in the UBL exists between locations. One instance of this spatial variability is vertical mixing; the Bronx site appears to have stronger vertical mixing as shown in Figure 4, as  $\theta$  remains constant for a greater height than at the Queens and Staten Island locations, indicating a deeper mixed layer. This phenomenon is more pronounced during extreme heat events, as a distinct mixed layer is apparent in the Bronx during early (12:00 LST) and late (18:00 LST) afternoon hours. While a deepened mixed layer during extreme heat events is also visible for the other locations, the strength of vertical mixing in the Bronx is emphasized by persistent afternoon instability as shown by negative  $\frac{d\theta}{dz}$  values between 500 and 1000 m and a superadiabatic surface layer and 12:00 and 18:00 LST. The area around the Bronx station is relatively more urbanized compared to the other 2 sites. The majority of the buildings are low- and medium-rise residential buildings and the average building height is 9.23 m compared to 6.22 m and 5.24 m at Queens and Staten Island, respectively (see Table 1). The increased roughness likely contributes to enhanced mixing within the boundary layer.

## 3.2 Moisture

On average, extreme heat events were found to increase the moisture at the surface, as indicated by the diurnal profiles of specific humidity ( $q$ ) (see Figure 3). This is also consistent across all observed locations in New York City, with mean extreme heat event  $q$  exceeding normal  $q$  by approximately  $1\text{-}\sigma$  over the entire day. Although a distinct diurnal profile exists ( $q$  decreases during daytime hours), the diurnal range is smaller in magnitude than temperature. It is also worth noting that the diurnal range is lower for Staten Island than for the Bronx or Queens, suggesting that degree of urbanization has a negative correlation with the diurnal range of  $q$ , due to sustained low-level moisture from local evapotranspiration from nearby vegetated areas. Similar to surface temperature, the variability of  $q$  is significantly lower during heat events (average  $\sigma = 2.14 \times 10^{-3} \text{ kg kg}^{-1}$ ) than during normal temperatures (average  $\sigma = 3.18 \times 10^{-3} \text{ kg kg}^{-1}$ ). Queens shows exceptional variability in  $q$ , which may be attributed to the location of the observation site, which is adjacent to Flushing Meadows Corona Park (large open vegetated space), is surrounded by a medium-density urban area on all other sides, and is approximately 4 km from Long Island Sound.

In the boundary layer, the positive  $q$  anomalies subside in magnitude between 300 and 600 m, but increase significantly in the mixed layer, especially during the late morning and early afternoon for all sites. As shown in Figure 2, the largest anomalies occur between 10:00 and 16:00 LST throughout the mixed layer. With regards to spatial variation in  $q$ , Staten Island demonstrates a strong positive anomaly overnight through the early morning near the surface, indicating increased low-level moisture transport during extreme heat events, whereas the Bronx and Queens demonstrate a similar phenomenon

with a lesser anomaly magnitude. All sites show significant positive  $q$  anomalies throughout the day, with the strongest anomaly signal starting in the low-levels throughout the morning and transitioning to the mixed later by mid-afternoon. This trend suggests that the increase in nocturnal low-level moisture corresponds to increased UBL moisture content due to strong vertical mixing throughout the daytime.

This is supported by Figure 5, where vertical profiles of  $q$  across all locations show markedly higher  $q$  values at the surface during extreme heat events (approximately  $1-\sigma$ ), with  $\frac{dq}{dz}$  values increasing throughout the morning in the mixed layer while low-level  $q$  values decrease, indicating vertical transport of moisture and drier low-level conditions during peak insolation. The strong vertical mixing of  $q$  can be observed at all sites, where late morning and early afternoon  $\frac{dq}{dz}$  values are greater during extreme heat events than normal days. An example can be seen in the Bronx, where  $\frac{dq}{dz} > 0$ , indicating very efficient vertical moisture transport.

In addition to environmental contributions to the positive  $q$  anomalies during extreme heat events, it is known that anthropogenic contribution of water vapor increases during extreme heat periods. In New York City, most commercial buildings use chilled water coolers for air conditioning. For example, Gutiérrez et al. (2015) found significant contributions from the air conditioning system to atmospheric water vapor in the lower boundary layer. Similar findings were observed in Beijing (M. Yu et al., 2019) and Hong Kong (Y. Wang et al., 2018).

### 3.3 UBL dynamics

#### 3.3.1 Horizontal winds

Extreme heat events coincided with a modest reduction of horizontal wind speeds ( $U$ ) in the UBL, as shown in Figure 3. More specifically, the magnitude of  $U$  during extreme heat events is similar in magnitude to  $U$  during normal days with the exception of early morning hours and at upper levels of the UBL. As shown in Figure 2, modest reductions in  $U$  ( $-1.2 \leq \sigma \leq -0.4$ ) during extreme heat events are present throughout the UBL from early to mid-morning, with little difference throughout the rest of the day ( $-0.4 \leq \sigma \leq 0.4$ ). Larger deviations between  $U$  values are present at the top of the UBL where synoptic conditions become dominant.

Vertical profiles of  $U$  for normal and extreme heat events at specific hours provide a more detailed view of the differences in UBL structure. Across all sites,  $U$  is similar throughout the UBL during afternoon, evening, and overnight hours. During early morning hours, however, extreme heat event  $U$  values decrease by 25 to 50% throughout the entire UBL (see Figure 6), although both event types present a classical logarithmic wind profile, with surface friction effects present through 500 m. The reduction in  $U$  during extreme heat events is likely due to the presence of an anticyclonic circulation that suppresses the nocturnal low-level jet over New York City (T. C. Chen and Kpaeyeh, 1993). Another phenomenon worth noting is the difference in  $U$  profiles above 2000 m; profiles of  $U$  during extreme heat events are more consistent both vertically and spatially (between sites) than during normal days. This phenomenon demonstrates the effect of synoptic meteorological conditions on  $U$ , as the UBL typically remains below 2500 m. During extreme heat events, anticyclonic conditions produce more consistent atmospheric conditions relative to normal days, resulting in less variability between heat events than during normal days.

Extreme heat events result in a southwesterly shift in  $U$  throughout the UBL. This shift is present most evidently closer to the surface, as shown in Figures 7, 8, and 9, with winds at 100 m coming primarily from the southwest quadrant. All sites also present secondary maxima with winds approaching from the south and southeast, which suggests effects from the Atlantic sea breeze (effects from the sea breeze will be further discussed in Section 4). At 1000 m, the directionality of prevailing winds becomes more uniform between normal and extreme heat days, as winds primarily approach New York City from the



west-southwest. The disparity in wind directions between 100 and 1000 m suggests that localized wind fields play a more significant role in UBL dynamics at lower levels whereas synoptic-scale atmospheric conditions increasingly dominate with increasing height. Regardless, the uniformity of wind direction during extreme heat relative to normal days indicates that synoptic-scale effects can play a larger role at lower levels due to advection from the continent, especially with regards to thermal advection that leads to the transport of heated inland air masses over New York City (Jiang et al., 2019; Ramamurthy et al., 2017).

### 3.3.2 Vertical motion

On average, extreme heat events do not appear to produce significant changes in vertical velocity ( $w$ ) relative to normal days. Figure 3 shows average diurnal profiles of  $w$  at all locations at 100 m above ground level, with similar mean values throughout the day between normal days and extreme heat events. During extreme heat events, the variability of  $w$  is lesser in the early morning hours and greater in the evening, albeit featuring similar behavior to normal days. This phenomenon is also observed in vertical profiles of  $w$  at all locations as shown in Figure 10. At all locations, overnight and morning profiles of  $w$  (0:00 and 6:00 LST) show significantly lower variability in  $w$  throughout the UBL with similar magnitudes of mean  $w$ , although extreme heat days feature low variability in the UBL. Despite similar means and deviations in the early afternoon (12:00 LST), evening profiles (18:00 LST) show significantly higher variability in  $w$  below 500 m than in the mornings at the Queens and Staten Island sites, with the Bronx showing this occurrence extend through the UBL. The similarity in vertical profiles of  $w$  may be a result of a balance between large-scale subsidence (due to the presence of high-pressure during extreme heat events) and the effects of increased surface forcings during extreme heat events relative to normal days (Dong et al., 2018; D.-L. Zhang et al., 2009).

Additionally, updrafts appear to be lesser in magnitude relative to normal days, although upwards vertical motion persists later at all heights within the UBL. This suggests that vertical mixing is more sustained throughout the day during extreme heat events, although thermal plumes seem to be weaker relative to normal days. A case of this is shown at the Bronx site (see Figure 11), where two days - 26 July 2019 (normal) and 29 July 2019 (extreme heat) - are shown with significantly different temporal profiles. On 26 July, the morning UBL is shallow and neutral through 10:00 LST, where mixing begins as evidenced by surface layer variability in  $w$ , which is followed by a sustained downdraft throughout the mixed layer. At approximately 12:00 LST, a strong plume extends throughout the UBL, initiating significant mixing from the surface throughout the mixed layer. This is followed by modest downdrafts throughout the UBL in the afternoon, followed by relatively neutral conditions in the evening and early nighttime hours. In contrast, 29 July demonstrates similar UBL dynamics in the morning hours, followed by modest low-level mixing through the midday hours, with sustained upwards vertical motions through the afternoon and evening over the entire UBL.

## 4 Effects of the sea breeze circulation

Sea breezes in New York City occur as a result of land-sea temperature gradients from two arms of the Atlantic Ocean; the New York Bight to the southeast and Long Island Sound to the northeast. Sea breezes from both bodies increase the complexity of UBL dynamics over New York City due to the coalescence of opposing fronts over the complex urban topography (Bornstein and Thompson, 1981). A typical sea breeze event in New York City is defined by calm ambient low-level winds ( $\leq 5 \text{ m s}^{-1}$ ), the formation of a large land-sea temperature gradient in the mid- to late morning, strong late-morning thermals that promote low-level convergence, and afternoon to early-evening onshore moisture transport and reduction in surface air temperatures (especially in areas closest to the shore) (Childs and Raman, 2005; Frizzola and Fisher, 1963; Gedzelman et al., 2003).

396

397 Sea breeze events occurred on approximately 56% of all days observed. The high frequency of  
 398 occurrence is attributable to low-level convergence due to the large land-sea temperature gradient  
 399 that is common during warmer months (Childs and Raman, 2005; Gedzelman et al., 2003; Thompson  
 400 et al., 2007), as days were chosen exclusively between May and September. Maximum land-sea surface  
 401 temperature differences during days with identifiable sea breeze events averaged at 12 K, with a strong  
 402 diurnal profile with the peak difference occurring around midday (see Figure 12). The frequency of  
 403 occurrence increases when observing days during extreme heat events, as the lack of a strong synoptic  
 404 wind allows for the sea breeze circulation to become dominant in the metropolitan area (Miller et al.,  
 405 2003).

#### 406 4.1 UBL structure during sea breeze events

407 During normal days, observations show that the sea breeze reduces temperature and increases moisture  
 408 content throughout the UBL after 12:00 LST. In Figure 13, the standardized anomalies of  $\theta$  between  
 409 normal days with and without a sea breeze are shown, averaged over all days on an hourly basis.  
 410 Overnight and in the early morning, positive anomalies of  $\theta$  are present above the UBL ( $\geq 1$  km)  
 411 until mid-morning, with the Bronx having the most significant anomaly and Staten Island the least.  
 412 This suggests a decreasing degree of anomalous  $\theta$  with decreasing urbanization. This anomaly pattern  
 413 coincides with a positive  $q$  anomaly trend in both the spatiotemporal aspect (peak anomaly occurs  
 414 above 1 km before 8:00 LST) and the magnitude aspect (the Bronx has the most significant early  
 415 morning anomaly, Staten Island has the least). Later in the day, all sites observe a negative  $\theta$  anomaly  
 416 throughout the UBL despite a negative  $q$  anomaly, indicating that sea breeze events during normal days  
 417 coincide with a cooler and drier daytime UBL before the onset of the sea breeze. Sea breeze effects  
 418 become apparent during the mid-afternoon with the presence of a significant negative  $\theta$  and positive  
 419  $q$  anomaly in the lower UBL, with Staten Island experiencing effects first (approximately 16:00 LST)  
 420 and the Bronx experiencing effects last (approximately 19:00 LST). This disparity in times appears to  
 421 represent the passage of the southeasterly New York Bight, and to a lesser degree, the Long Island  
 422 Sound sea breeze fronts through New York City, where the onset time correlates with the distance from  
 423 the bodies of water (Bornstein and Thompson, 1981). It is worth noting that the  $q$  anomaly is weak-  
 424 est in the Bronx, which suggests that the sea breeze front weakens as it travels inland over New York City.

425

426 During extreme heat events, observations show that the sea breeze plays a moderating role on  
 427 surface conditions by reducing low-level temperatures and increasing low-level moisture content, similar  
 428 to phenomena observed during normal days. In Figure 14, the standardized anomalies of  $\theta$  between  
 429 extreme heat days with and without a sea breeze are shown, averaged over all days. All sites shown  
 430 that extreme heat days with a sea breeze possess slightly higher values of  $\theta$  in the mid-morning,  
 431 with significant low-level reduction in  $\theta$  in the afternoon and evening. On average, the onset of the  
 432 low-level cooling occurs in Staten Island first at approximately 12:00 LST, with Queens following at  
 433 approximately 14:00 LST, and the Bronx at about 18:00 LST. It is worth noting that the negative  $\theta$   
 434 anomalies are stronger in more urbanized areas, as shown by the Bronx and Queens sites. A similar  
 435 phenomenon is observed by the transport of  $q$  as shown in Figure 14, with drier conditions throughout  
 436 the UBL before 12:00 LST and increasing low-level moisture as the day progresses. With regards to  
 437 onset,  $q$  follows a similar pattern to  $\theta$  in that the onset time is dependent from distance to the shore.  
 438 These anomalies present most significantly in the lowest 1000 m of the UBL after 12:00 LST, which  
 439 aligns with sea breeze circulation characteristics observed in Frizzola and Fisher (1963).

#### 440 4.2 UBL dynamics during sea breeze events

441 Days with identifiable sea breeze events had lower  $U$  throughout the majority of the UBL, with the  
 442 most significant decreases during the nighttime, potentially due to the lessening of onshore flow due

to the reduction of the land-sea temperature gradient (Pullen et al., 2007), as shown in Figure 12. Vertical motions, however, increased significantly in the Bronx and Queens during the late morning and early afternoon, as shown in Figure 14. These anomalies indicate the increased presence of updrafts in urbanized areas which contribute to low-level convergence and the initiation of a localized sea breeze circulation, promoting onshore flow in the afternoon and evening.

During extreme heat days with identified sea breeze circulations, easterly winds increase in frequency in the lower levels of the UBL, as shown in Figure 15. These winds are the result of onshore flow from the New York Bight (southeasterly) and Long Island Sound (northeasterly).

During extreme heat days with sea breeze circulations, southeasterly winds increased in frequency compared to all other directions at all locations. The occurrence frequency of southeasterly winds is correlated with the distance between the observation site and the largest body of water in proximity of the metropolitan area (Atlantic Ocean), as Staten Island reported 92.1% of all winds at 100 m as southeasterly between 12:00 and 20:00 LST (distance of 6.50 km from Lower New York Bay), whereas Queens reported 67.4% (distance of 16.5 km) and Bronx reported 55.6% (distance of 32.9 km) during the same time interval. The disparity in southeasterly winds further demonstrates the spatial extent and progression of the sea breeze front.

For sites near Long Island Sound (the Bronx and Queens), northeasterly winds increased in frequency as well, though not to the same magnitude as southeasterly winds. This disparity in magnitude suggests that the Long Island Sound sea breeze front is weaker than the New York Bight sea breeze front, which aligns with previous studies of sea breeze fronts over New York City (Frizzola and Fisher, 1963; Meir et al., 2013). Northeasterly winds increased in frequency during extreme heat days with sea breeze circulations, with a notable increase in the early morning hours (a likely result of nocturnal low-level motion) and in the evening hours (signal of a Long Island Sound sea breeze). This phenomenon is also apparent in Queens and Staten Island, albeit to a lesser frequency.

## 5 Discussion and conclusions

Several phenomena observed in this study have been noted in the literature. With regards to heat-related phenomena, the 'heat dome' effect observed through comprehensive multi-city airborne observations in Y. Zhang et al. (2020) was observed herein, with a notable increase in temperatures ( $\sigma \geq 0.99$ ) throughout the UBL during extreme heat events. Specifically, the peak temperature anomalies during extreme heat events occurred during the early morning and early afternoon in the surface layer, with secondary maxima in the mixed layer at approximately 1500 m. This behavior is similar to meteorological conditions presented by Ortiz et al. (2018) from a series of factor-separation studies using the Weather Research and Forecasting (WRF) model to understand the effects of urbanization on meteorological conditions in New York City. The results showed that surface factors from urban land cover types presented substantial increases to the surface and mixed layer temperatures (6 to 8 K throughout the day). Moreover, simulations showed especially robust early morning (6:00 LST) mixed layer increases in  $\theta$  during extreme heat events, which aligns with composite observations shown herein, despite the studies only ranging over a 5-day period for a specific extreme heat event.

With regards to moisture-related phenomena, several studies have shown that there is increased UBL moisture content during extreme heat events (Kunkel et al., 1996; Pyrgou et al., 2020; Y. Zhang et al., 2020). In particular, the positive anomalies of  $q$  are strongest in the surface layer during the morning, which aligns with findings from the Midwestern United States (Kunkel et al., 1996) and various regions of differing climates (Y. Zhang et al., 2020). Y. Zhang et al. (2020) also presented comparisons of the average diurnal vertical structure of  $q$  in humid regions (Louisville, Houston, and Philadelphia) and

an inland city in a dry inland region (Denver) and showed the differences in the UBL  $q$ . Louisville and Philadelphia experienced increases in  $q$  throughout the UBL, whereas Houston and Denver experienced decreases in low-level  $q$ , despite Houston being a coastal city in a humid region. This phenomenon was attributed to synoptic-scale moisture transport, where moist air masses from surrounding humid areas paired with local evapotranspiration to increase  $q$  in Louisville and Philadelphia, but drier air masses from the Mountain West resulted in lower  $q$  values during extreme heat events. The effects of extreme heat on  $q$  in New York City resemble those of the cities in humid regions, where humid continental air masses paired with evapotranspiration from vegetated areas surrounding the area to increase  $q$  substantially ( $0.1 \leq \sigma \leq 1.2$ ). The influence of localized UBL dynamics (i.e., sea breeze) further increased low-level  $q$  as a result of onshore moisture transport, especially during nighttime hours.

On a larger scale, differences in UBL dynamics have been shown to play a major factor in UBL properties between normal and extreme heat days. As shown herein, a southwesterly shift in winds throughout the UBL coincided with extreme heat events, further highlighting the role of synoptic conditions on the UBL during extreme heat. The increase in temperatures due to this shift in winds has been reported in multiple studies (Heaviside et al., 2015; Jiang et al., 2019; Ramamurthy et al., 2017), where the shift in wind direction results in advection of hot air from continental land masses or the advection of heat from nearby urban areas. In the case of New York City, a southwesterly shift in winds places New York City downwind of the continental United States and the north-central New Jersey urban conurbation, both of which may contribute to a hotter UBL during extreme heat events. Moreover, the effect of sea breezes from multiple fronts around New York City creates a complex flow pattern that increases spatial variability in the local meteorology, which has been shown to reduce temperature throughout the UBL (Han et al., 2022; Hirsch et al., 2021; Lee et al., 2021), albeit contributing to higher moisture content which affects the nocturnal and successive morning UBL structure.

Despite the extensive results provided herein, additional work is required to better improve our understanding of neighborhood-scale spatial qualities of the boundary layer throughout urban areas, especially in those with complex topography and land cover attributes, such as a coastal city. Despite observation sites in 3 of the 5 boroughs, New York City also features a highly variable array of land cover types and features that are not represented in this study. For example, targeting areas in the densest parts of the city (e.g., Midtown Manhattan) or furthest from the coast (e.g., central Brooklyn) would be ideal for observing UBL properties in areas of the city most likely to have peak surface temperatures. The variability of building heights throughout New York City, especially in Manhattan, further complicates UBL dynamics and downwind transport (S. Hanna et al., 2007; S. R. Hanna et al., 2006). Moreover, the distance between sites is on the order of the size of a borough, rendering each station unable to be fully representative of neighborhood-scale processes. A potential solution includes a more extensive network of weather and profiling stations (the Oklahoma City Micronet and its usage as described by Basara et al. (2010) is a useful example) that allows for more land cover types to be represented.

Based on the observations and their derived quantities, insight was provided into the questions posed in Section 1;

1. Regarding UBL structure, the UBL shows increased temperatures and moisture content throughout its entirety during extreme heat events. Specifically, the surface and lower mixed layer show the most significant increases in temperature and moisture throughout the diurnal cycle. Moreover, the afternoon mixed layer presents a secondary maxima in temperature and moisture increases, suggesting more sustained vertical mixing during extreme heat events. Regarding UBL dynamics, horizontal wind speeds are slightly lower on average during extreme heat events, with the most notable reductions present in the early morning hours and at the UBL height. Additionally,

the directionality of horizontal winds becomes predominantly southwesterly and uniform across the UBL during extreme heat events, suggesting increased low-level advection from the continental United States. Differences in vertical motions between normal days and days with extreme heat are not significant when averaged, although extreme heat events were found to correlate with weaker updrafts despite sustaining prolonged positive  $w$  values through the evening hours. Extreme heat days were also found to be less variable in terms of UBL structure and dynamics relative to normal days.

2. Locally, the transport of scalars appears to increase in the vertical direction during extreme heat events in the UBL, although decreased low-level horizontal winds suppresses strong scalar transport zonally and meridionally, especially during morning hours. Despite similar vertical rates of change of scalar quantities between normal days and days with extreme heat, the increase in low-level temperature and moisture content results in significantly higher mixed layer temperature and specific humidity values during extreme heat days. Moreover, extreme heat days appear to promote onshore low-level moisture transport, especially in areas immediately adjacent to the coast. This phenomenon coincides with an increased sea breeze event frequency during extreme heat events. On a larger scale, the vertical uniformity in wind direction throughout the UBL during extreme heat events promotes the advection of scalars southwest of New York City.
3. The sea breeze reduces temperatures throughout the UBL after the onset of the sea breeze, which typically occurs in the mid-afternoon in immediate coastal areas and in the evening for areas further inland. The sea breeze also results in nocturnal low-level onshore moisture transport. The effects of the sea breeze were evaluated for (a) normal days and (b) days with extreme heat. During (a) normal days with sea breezes, the effects of the sea breeze resulted in a reduction of low-level temperatures and an increase in moisture content throughout the UBL relative to normal days without a detectable sea breeze, especially after during the evening. During (b) extreme heat days with sea breezes, the effects of the sea breeze similarly resulted in a reduction of low-level temperatures and an increase in moisture content throughout the UBL relative to extreme heat days without a detectable sea breeze, especially after during the evening. It is worth noting that during normal days, there was no significant difference in vertical velocities during days with a sea breeze relative to days without a sea breeze, despite a significant reduction in horizontal winds. However, extreme heat days, significantly higher  $w$  values occurred through the surface and lower mixed layer during the late morning periods at the Bronx and Queens sites.

## Acknowledgments

This research is made possible by the New York State (NYS) Mesonet. Original funding for the NYS Mesonet was provided by Federal Emergency Management Agency grant FEMA-4085-DR-NY, with the continued support of the NYS Division of Homeland Security & Emergency Services; the state of New York; the Research Foundation for the State University of New York (SUNY); the University at Albany, SUNY; the Atmospheric Sciences Research Center (ASRC) at SUNY Albany; and the Department of Atmospheric and Environmental Sciences (DAES) at SUNY Albany. This research was also funded by the Department of Defense Army Research Office Grant No. W911NF2020126.

## References

- Anderson, G Brooke and Michelle L Bell (2011). “Heat waves in the United States: mortality risk during heat waves and effect modification by heat wave characteristics in 43 US communities”. In: *Environmental health perspectives* 119.2, pp. 210–218.

584 Anurose, TJ, D Bala Subrahmanyam, and SV Sunilkumar (2018). “Two years observations on the diurnal  
585 evolution of coastal atmospheric boundary layer features over Thiruvananthapuram (8.5° N, 76.9° E), India”.  
586 In: *Theoretical and applied climatology* 131.1, pp. 77–90.

587 Arruda Moreira, Gregori de et al. (2020). “Study of the planetary boundary layer height in an urban environment  
588 using a combination of microwave radiometer and ceilometer”. In: *Atmospheric Research* 240, p. 104932.

589 Banks, Robert F et al. (2015). “Performance evaluation of the boundary-layer height from lidar and the Weather  
590 Research and Forecasting model at an urban coastal site in the north-east Iberian Peninsula”. In: *Boundary-  
591 layer meteorology* 157.2, pp. 265–292.

592 Barlow, Janet F (2014). “Progress in observing and modelling the urban boundary layer”. In: *Urban Climate* 10,  
593 pp. 216–240.

594 Barlow, Janet F et al. (2011). “Boundary layer dynamics over London, UK, as observed using Doppler lidar  
595 during REPARTEE-II”. In: *Atmospheric Chemistry and Physics* 11.5, pp. 2111–2125.

596 Basara, Jeffrey B et al. (2010). “The impact of the urban heat island during an intense heat wave in Oklahoma  
597 City”. In: *Advances in Meteorology* 2010.

598 Bauer, Timothy J (2020). “Interaction of urban heat island effects and land–sea breezes during a New York City  
599 heat event”. In: *Journal of Applied Meteorology and Climatology* 59.3, pp. 477–495.

600 Best, MJ (2005). “Representing urban areas within operational numerical weather prediction models”. In:  
601 *Boundary-Layer Meteorology* 114.1, pp. 91–109.

602 Black, Emily et al. (2004). “Factors contributing to the summer 2003 European heatwave”. In: *Weather* 59.8,  
603 pp. 217–223.

604 Bornstein, Robert D and William T Thompson (1981). “Effects of frictionally retarded sea breeze and synoptic  
605 frontal passages on sulfur dioxide concentrations in New York City”. In: *Journal of Applied Meteorology and  
606 Climatology* 20.8, pp. 843–858.

607 Brotzge, Jerald A et al. (2020). “A technical overview of the new york state mesonet standard network”. In:  
608 *Journal of Atmospheric and Oceanic Technology* 37.10, pp. 1827–1845.

609 Bureau, United States Census (2021). *2020 Population and Housing State Data*. URL: [https://www.census.gov/  
610 library/visualizations/interactive/2020-population-and-housing-state-data.html](https://www.census.gov/library/visualizations/interactive/2020-population-and-housing-state-data.html).

611 Burillo, Daniel et al. (2019). “Electricity infrastructure vulnerabilities due to long-term growth and extreme heat  
612 from climate change in Los Angeles County”. In: *Energy Policy* 128, pp. 943–953.

613 Chen, Feng, Xuchao Yang, and Weiping Zhu (2014). “WRF simulations of urban heat island under hot-weather  
614 synoptic conditions: The case study of Hangzhou City, China”. In: *Atmospheric research* 138, pp. 364–377.

615 Chen, T C and J Alvin Kpaeyeh (1993). “The synoptic-scale environment associated with the low-level jet of the  
616 Great Plains”. In: *Monthly weather review* 121.2, pp. 416–420.

617 Childs, Peter P and Sethu Raman (2005). “Observations and numerical simulations of urban heat island and sea  
618 breeze circulations over New York City”. In: *Pure and Applied Geophysics* 162.10, pp. 1955–1980.

619 Colle, Brian A and David R Novak (2010). “The New York Bight jet: climatology and dynamical evolution”. In:  
620 *Monthly Weather Review* 138.6, pp. 2385–2404.

621 Davis, Edwin V, K Rajeev, and KV Sambhu Namboodiri (2021). “The Convective-Atmospheric-Boundary-Layer  
622 Height and its dependence upon Meteorological Variables At a Tropical Coastal Station during Onshore and  
623 Offshore Flows”. In: *Boundary-Layer Meteorology*, pp. 1–24.

624 Dong, Li et al. (2018). “The dynamical linkage of atmospheric blocking to drought, heatwave and urban heat  
625 island in southeastern US: A multi-scale case study”. In: *Atmosphere* 9.1, p. 33.

626 Edwards, John M et al. (2020). “Representation of boundary-layer processes in numerical weather prediction and  
627 climate models”. In: *Boundary-Layer Meteorology* 177.2, pp. 511–539.

628 Forzieri, Giovanni et al. (2018). “Escalating impacts of climate extremes on critical infrastructures in Europe”.  
629 In: *Global environmental change* 48, pp. 97–107.

630 Frizzola, John A and Edwin L Fisher (1963). “A series of sea breeze observations in the New York City area”.  
631 In: *Journal of Applied Meteorology and Climatology* 2.6, pp. 722–739.

632 Frumkin, Howard (2016). “Urban sprawl and public health”. In: *Public health reports*.

633 Gedzelman, SD et al. (2003). “Mesoscale aspects of the urban heat island around New York City”. In: *Theoretical  
634 and applied climatology* 75.1, pp. 29–42.

635 González, Jorge E et al. (2021). “Urban climate and resiliency: A synthesis report of state of the art and future  
636 research directions”. In: *Urban Climate* 38, p. 100858.

637 Grund, Christian J et al. (2001). “High-resolution Doppler lidar for boundary layer and cloud research”. In:  
638 *Journal of Atmospheric and Oceanic Technology* 18.3, pp. 376–393.



- Güldner, J and D Spänkuch (2001). "Remote sensing of the thermodynamic state of the atmospheric boundary layer by ground-based microwave radiometry". In: *Journal of Atmospheric and Oceanic Technology* 18.6, pp. 925–933.
- Gutiérrez, Estatio et al. (2015). "On the anthropogenic heat fluxes using an air conditioning evaporative cooling parameterization for mesoscale urban canopy models". In: *Journal of Solar Energy Engineering* 137.5.
- Han, ZS et al. (2022). "Observed sea breeze life cycle in and around NYC: Impacts on UHI and ozone patterns". In: *Urban Climate* 42, p. 101109.
- Hanna, Steven, John White, and Ying Zhou (2007). "Observed winds, turbulence, and dispersion in built-up downtown areas of Oklahoma City and Manhattan". In: *Boundary-layer meteorology* 125.3, pp. 441–468.
- Hanna, Steven R et al. (2006). "Detailed simulations of atmospheric flow and dispersion in downtown Manhattan: An application of five computational fluid dynamics models". In: *Bulletin of the American Meteorological Society* 87.12, pp. 1713–1726.
- Heaviside, Clare, X-M Cai, and SJQJotRMS Vardoulakis (2015). "The effects of horizontal advection on the urban heat island in Birmingham and the West Midlands, United Kingdom during a heatwave". In: *Quarterly Journal of the Royal Meteorological Society* 141.689, pp. 1429–1441.
- Heaviside, Clare, Helen Macintyre, and Sotiris Vardoulakis (2017). "The urban heat island: implications for health in a changing environment". In: *Current environmental health reports* 4.3, pp. 296–305.
- Hewison, Tim and Catherine Gaffard (2003). "Radiometrics MP3000 microwave radiometer performance assessment". In: *Obs. Development Technical Report TR29, Met Office, National Meteorological Library, Exeter, UK. Also available from <http://tim.hewison.org/TR29.pdf>*.
- Hirsch, Annette L et al. (2021). "Resolving the influence of local flows on urban heat amplification during heatwaves". In: *Environmental Research Letters* 16.6, p. 064066.
- Hrisko, Joshua, Prathap Ramamurthy, and Jorge E Gonzalez (2021). "Estimating heat storage in urban areas using multispectral satellite data and machine learning". In: *Remote Sensing of Environment* 252, p. 112125.
- Hu, Xiao-Ming and Ming Xue (2016). "Influence of synoptic sea-breeze fronts on the urban heat island intensity in Dallas–Fort Worth, Texas". In: *Monthly Weather Review* 144.4, pp. 1487–1507.
- Ignatov, A et al. (2010). "GOES-R Advanced Baseline Imager (ABI) algorithm theoretical basis document for sea surface temperature". In: *NOAA NESDIS Center for Satellite Applications and Research*.
- Jiang, Shaojing et al. (2019). "Amplified urban heat islands during heat wave periods". In: *Journal of Geophysical Research: Atmospheres* 124.14, pp. 7797–7812.
- Kumer, Valerie-M, Joachim Reuder, and Birgitte R Furevik (2014). "A comparison of LiDAR and radiosonde wind measurements". In: *Energy Procedia* 53, pp. 214–220.
- Kunkel, Kenneth E et al. (1996). "The July 1995 heat wave in the Midwest: A climatic perspective and critical weather factors". In: *Bulletin of the American Meteorological Society* 77.7, pp. 1507–1518.
- Lee, Young-Hee, Moon-Soo Park, and Yuna Choi (2021). "Planetary Boundary-Layer Structure at an Inland Urban Site under Sea Breeze Penetration". In: *Asia-Pacific Journal of Atmospheric Sciences* 57.4, pp. 701–715.
- Leroyer, Sylvie et al. (2014). "Subkilometer numerical weather prediction in an urban coastal area: A case study over the Vancouver metropolitan area". In: *Journal of Applied Meteorology and Climatology* 53.6, pp. 1433–1453.
- Li, Dan and Elie Bou-Zeid (2013). "Synergistic interactions between urban heat islands and heat waves: The impact in cities is larger than the sum of its parts". In: *Journal of Applied Meteorology and Climatology* 52.9, pp. 2051–2064.
- Luo, Bingkun and Peter J Minnett (2021). "Skin Sea Surface Temperatures From the GOES-16 ABI Validated With Those of the Shipborne M-AERI". In: *IEEE Transactions on Geoscience and Remote Sensing* 59.12, pp. 9902–9913.
- Madrigano, Jaime et al. (2015). "A case-only study of vulnerability to heat wave-related mortality in New York City (2000–2011)". In: *Environmental health perspectives* 123.7, pp. 672–678.
- McEvoy, Darryn, Iftexhar Ahmed, and Jane Mullett (2012). "The impact of the 2009 heat wave on Melbourne's critical infrastructure". In: *Local Environment* 17.8, pp. 783–796.
- Meir, Talmor et al. (2013). "Forecasting the New York City urban heat island and sea breeze during extreme heat events". In: *Weather and Forecasting* 28.6, pp. 1460–1477.
- Melecio-Vázquez, David et al. (2018). "Thermal Structure of a Coastal–Urban Boundary Layer". In: *Boundary-Layer Meteorology* 169 (1), pp. 151–161. ISSN: 15731472.
- Miller, STK et al. (2003). "Sea breeze: Structure, forecasting, and impacts". In: *Reviews of geophysics* 41.3.

- Miralles, Diego G et al. (2014). “Mega-heatwave temperatures due to combined soil desiccation and atmospheric heat accumulation”. In: *Nature geoscience* 7.5, pp. 345–349.
- National Weather Service, NOAA (May 2018). *National Weather Service New York, NY excessive heat page*. URL: <https://www.weather.gov/okx/excessiveheat>.
- NOAA et al. (1998). *Automated Surface Observing System (ASOS) User’s Guide*. URL: <https://www.weather.gov/media/asos/aum-toc.pdf>.
- Ortiz, Luis E et al. (2018). “New York City impacts on a regional heat wave”. In: *Journal of applied meteorology and climatology* 57.4, pp. 837–851.
- Pelliccioni, A et al. (2012). “Some characteristics of the urban boundary layer above Rome, Italy, and applicability of Monin–Obukhov similarity”. In: *Environmental fluid mechanics* 12.5, pp. 405–428.
- Peng, Roger D et al. (2011). “Toward a quantitative estimate of future heat wave mortality under global climate change”. In: *Environmental health perspectives* 119.5, pp. 701–706.
- Pullen, Julie et al. (2007). “Atmospheric response to local upwelling in the vicinity of New York–New Jersey harbor”. In: *Journal of applied meteorology and climatology* 46.7, pp. 1031–1052.
- Pyrgou, Andri, Panos Hadjinicolaou, and Mat Santamouris (2020). “Urban-rural moisture contrast: Regulator of the urban heat island and heatwaves’ synergy over a mediterranean city”. In: *Environmental Research* 182, p. 109102.
- Quan, Jiannong et al. (2013). “Evolution of planetary boundary layer under different weather conditions, and its impact on aerosol concentrations”. In: *Particuology* 11.1, pp. 34–40.
- Ramamurthy, P and E Bou-Zeid (2017). “Heatwaves and urban heat islands: a comparative analysis of multiple cities”. In: *Journal of Geophysical Research: Atmospheres* 122.1, pp. 168–178.
- Ramamurthy, P, D Li, and E Bou-Zeid (2017). “High-resolution simulation of heatwave events in New York City”. In: *Theoretical and applied climatology* 128.1, pp. 89–102.
- Ramamurthy, Prathap and E Bou-Zeid (2014). “Contribution of impervious surfaces to urban evaporation”. In: *Water Resources Research* 50.4, pp. 2889–2902.
- Ramamurthy, Prathap et al. (2017). “Impact of heatwave on a megacity: an observational analysis of New York City during July 2016”. In: *Environmental Research Letters* 12.5, p. 054011.
- Robinson, Peter J (2001). “On the definition of a heat wave”. In: *Journal of Applied Meteorology and Climatology* 40.4, pp. 762–775.
- Ronda, RJ et al. (2017). “Urban finescale forecasting reveals weather conditions with unprecedented detail”. In: *Bulletin of the American Meteorological Society* 98.12, pp. 2675–2688.
- Rose, Thomas et al. (2005). “A network suitable microwave radiometer for operational monitoring of the cloudy atmosphere”. In: *Atmospheric research* 75.3, pp. 183–200.
- Roth, Matthias (2000). “Review of atmospheric turbulence over cities”. In: *Quarterly Journal of the Royal Meteorological Society* 126.564, pp. 941–990.
- Sánchez, JL et al. (2013). “A method to improve the accuracy of continuous measuring of vertical profiles of temperature and water vapor density by means of a ground-based microwave radiometer”. In: *Atmospheric Research* 122, pp. 43–54.
- Shreevastava, Anamika et al. (2021). “Scale-dependent response of the urban heat island to the European heatwave of 2018”. In: *Environmental Research Letters* 16.10, p. 104021.
- Shrestha, Bhupal et al. (2021). “Overview and Applications of the New York State Mesonet Profiler Network”. In: *Journal of Applied Meteorology and Climatology* 60.11, pp. 1591–1611.
- Stéfanon, Marc et al. (2014). “Soil moisture-temperature feedbacks at meso-scale during summer heat waves over Western Europe”. In: *Climate dynamics* 42.5, pp. 1309–1324.
- Tewari, Mukul et al. (2019). “Interaction of urban heat islands and heat waves under current and future climate conditions and their mitigation using green and cool roofs in New York City and Phoenix, Arizona”. In: *Environmental Research Letters* 14.3, p. 034002.
- Thomas, Natalie P et al. (2020). “Mechanisms associated with daytime and nighttime heat waves over the contiguous united states”. In: *Journal of Applied Meteorology and Climatology* 59.11, pp. 1865–1882.
- Thompson, William T, Teddy Holt, and Julie Pullen (2007). “Investigation of a sea breeze front in an urban environment”. In: *Quarterly Journal of the Royal Meteorological Society: A journal of the atmospheric sciences, applied meteorology and physical oceanography* 133.624, pp. 579–594.
- Wang, Y et al. (2018). “Effects of anthropogenic heat due to air-conditioning systems on an extreme high temperature event in Hong Kong”. In: *Environmental Research Letters* 13.3, p. 034015.

748 Wang, Z et al. (2012). “Lidar measurement of planetary boundary layer height and comparison with microwave  
749 profiling radiometer observation”. In: *Atmospheric Measurement Techniques* 5.8, pp. 1965–1972.

750 Wu, Yonghua et al. (2019). “Observation of heat wave effects on the urban air quality and PBL in New York  
751 City area”. In: *Atmospheric Environment* 218, p. 117024.

752 Yu, Miao et al. (2019). “On the assessment of a cooling tower scheme for high-resolution numerical weather  
753 modeling for urban areas”. In: *Journal of Applied Meteorology and Climatology* 58.6, pp. 1399–1415.

754 Yu, Yunyue et al. (2008). “Developing algorithm for operational GOES-R land surface temperature product”. In:  
755 *IEEE Transactions on Geoscience and Remote Sensing* 47.3, pp. 936–951.

756 Zhang, Da-Lin, Yi-Xuan Shou, and Russell R Dickerson (2009). “Upstream urbanization exacerbates urban heat  
757 island effects”. In: *Geophysical Research Letters* 36.24.

758 Zhang, Yuanjie et al. (2020). “Aircraft observed diurnal variations of the planetary boundary layer under heat  
759 waves”. In: *Atmospheric Research* 235, p. 104801.

760 Zhao, Lei et al. (2018). “Interactions between urban heat islands and heat waves”. In: *Environmental research  
761 letters* 13.3, p. 034003.

762 Zuo, Jian et al. (2015). “Impacts of heat waves and corresponding measures: a review”. In: *Journal of Cleaner  
763 Production* 92, pp. 1–12.

## 764 Appendix

$$p = p_0 \exp \frac{-gz}{RT_0}$$

$$\theta = T \left( \frac{p_0}{p} \right)^{\frac{R}{c_p}}$$

$$q = \frac{w}{1 + w} = \frac{\frac{\varepsilon \rho'_v R_v T}{p - \rho'_v R_v T}}{1 + \frac{\varepsilon \rho'_v R_v T}{p - \rho'_v R_v T}}$$

$$Ri_b = \frac{g \Delta \bar{\theta}_v \Delta z}{\bar{\theta}_v [(\Delta \bar{U}^2) + (\Delta \bar{V}^2)]}$$

Table 2: Symbols and abbreviations used in the paper.

Symbol/Abbreviation	Definition
$\sigma$	Standard deviation
$\theta$	Potential temperature
$q$	Specific humidity
$U$	Horizontal wind speed
$w$	Vertical velocity
UBL	Urban boundary layer
MLH	Mixed layer height

## 766 Figures

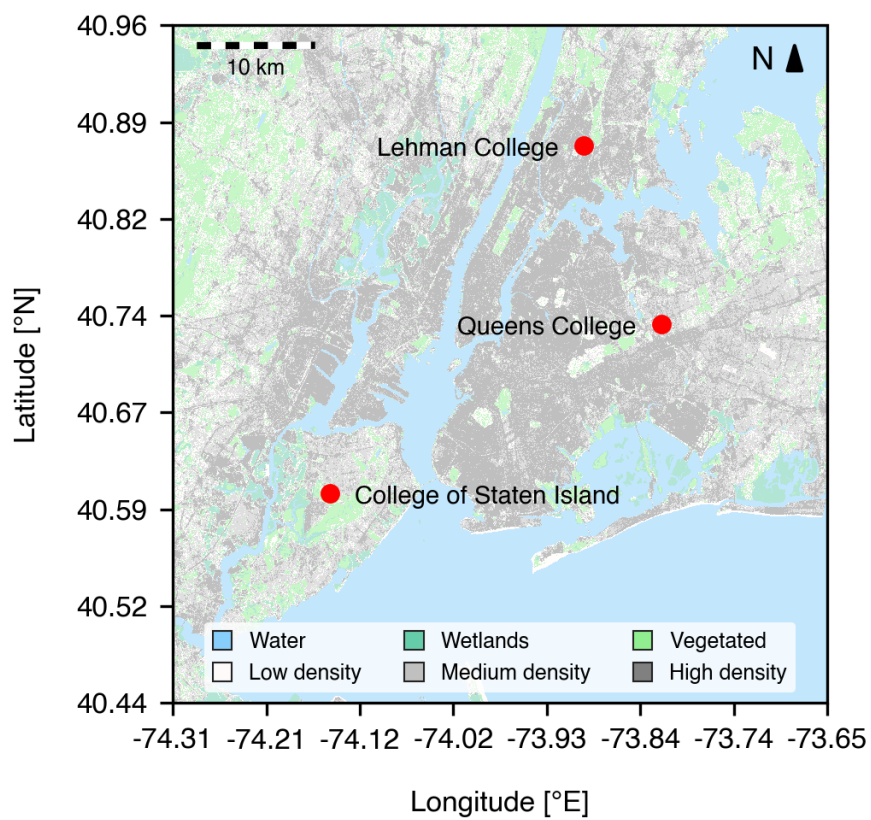


Figure 1: Observation sites overlaid on NLCD land cover types.

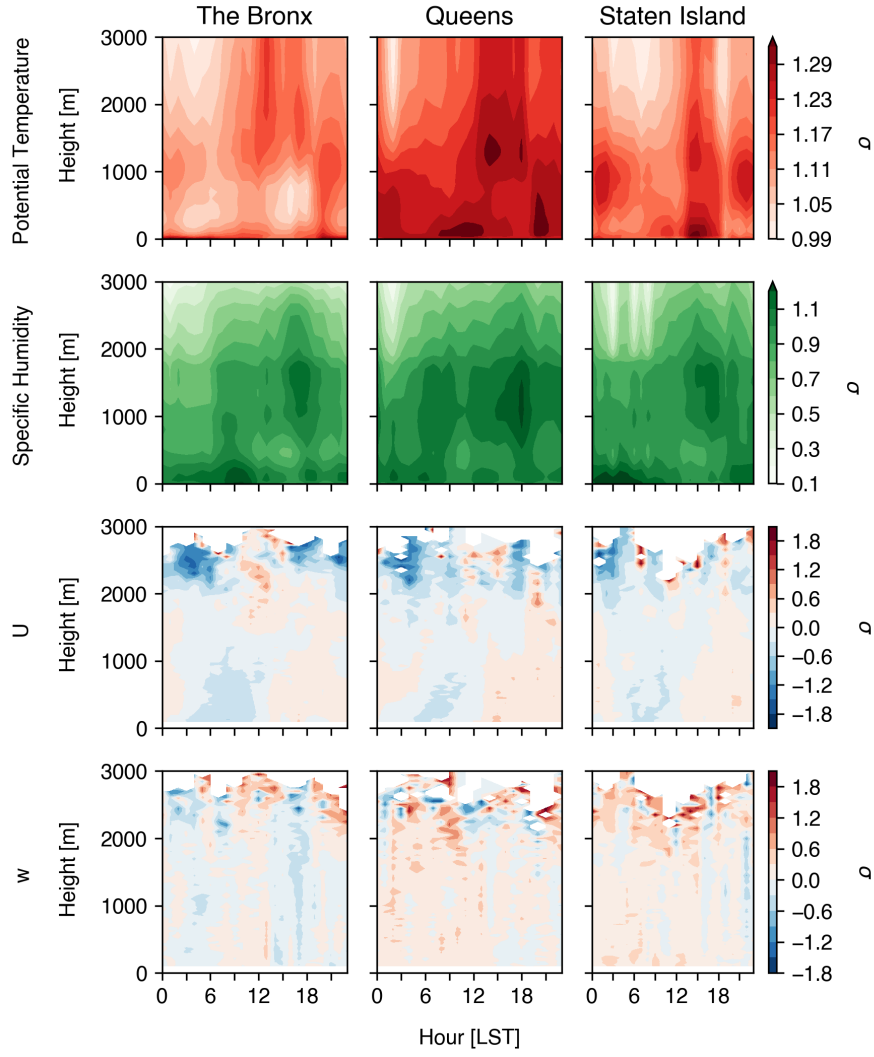


Figure 2: Anomalies during extreme heat events relative to the climatology over the urban boundary layer.

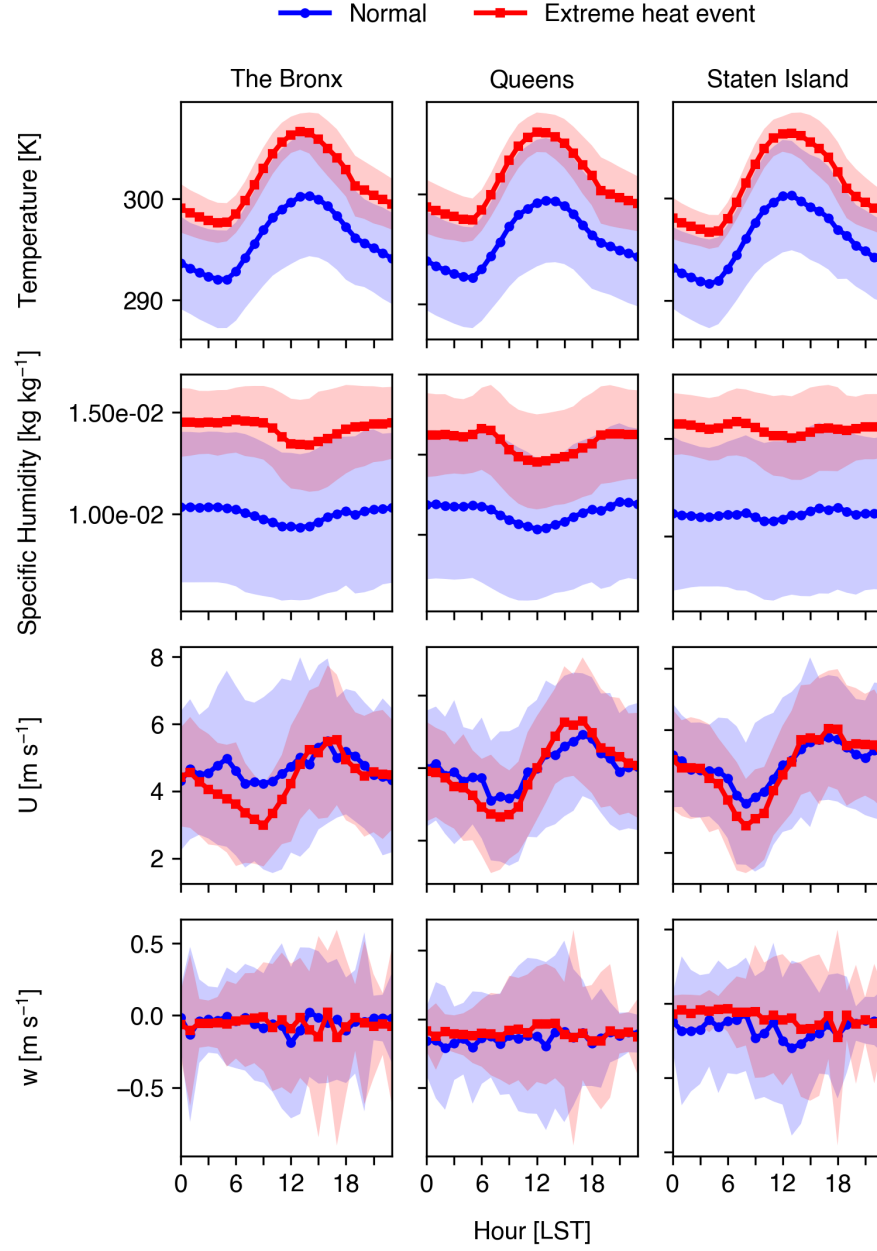


Figure 3: Anomalies of temperature during extreme heat events relative to the climatology at the surface.



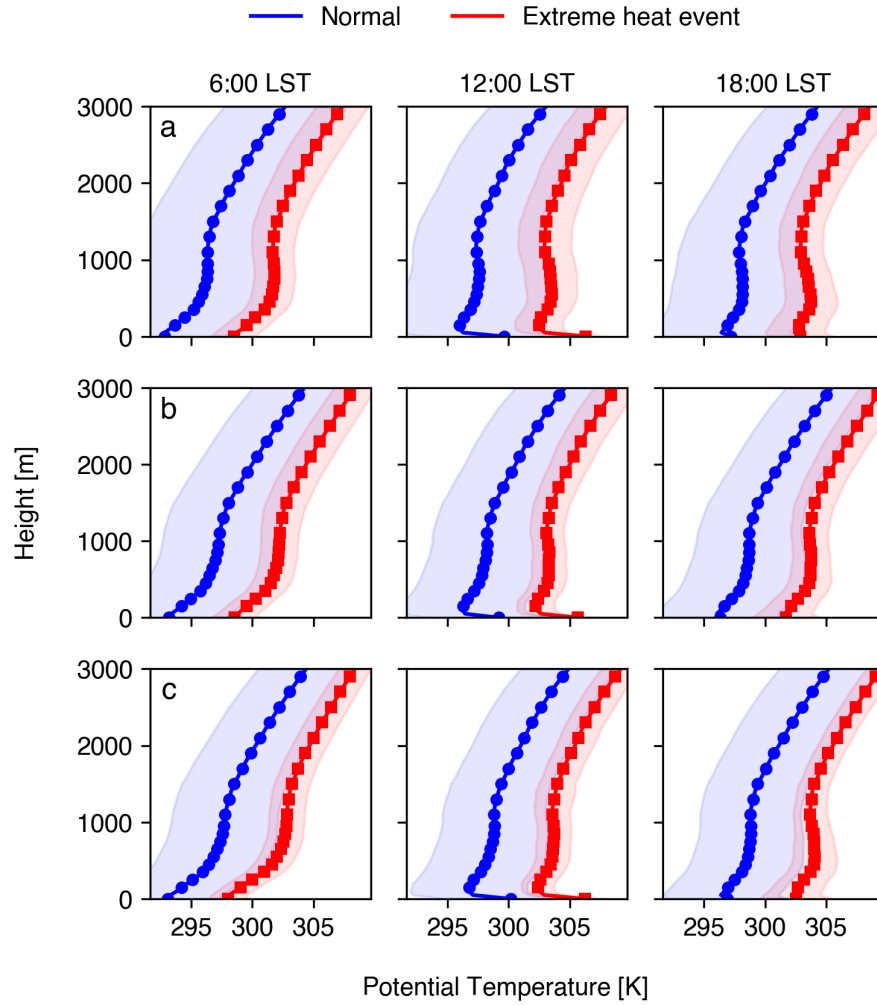


Figure 4: Vertical profiles of  $\theta$  at the Bronx (a), Queens (b), and Staten Island (c) sites during normal days (blue) and extreme heat events (red).

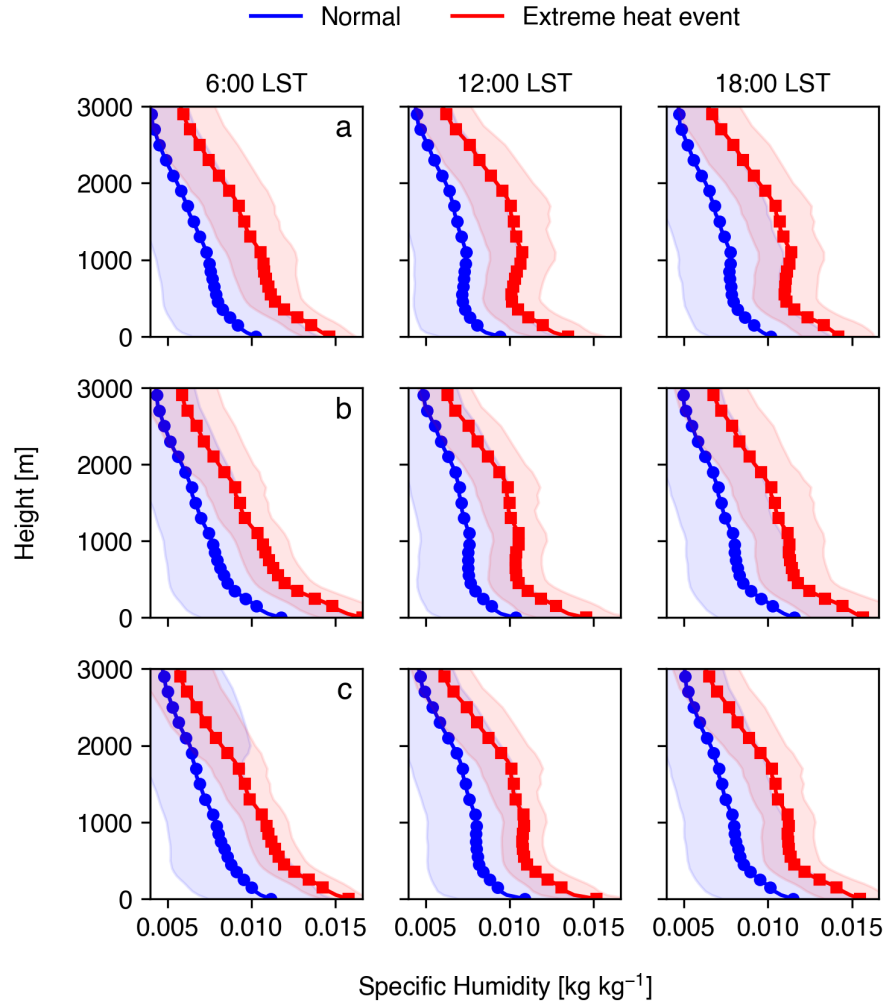


Figure 5: Vertical profiles of  $q$  at the Bronx (a), Queens (b), and Staten Island (c) sites during normal days (blue) and extreme heat events (red).

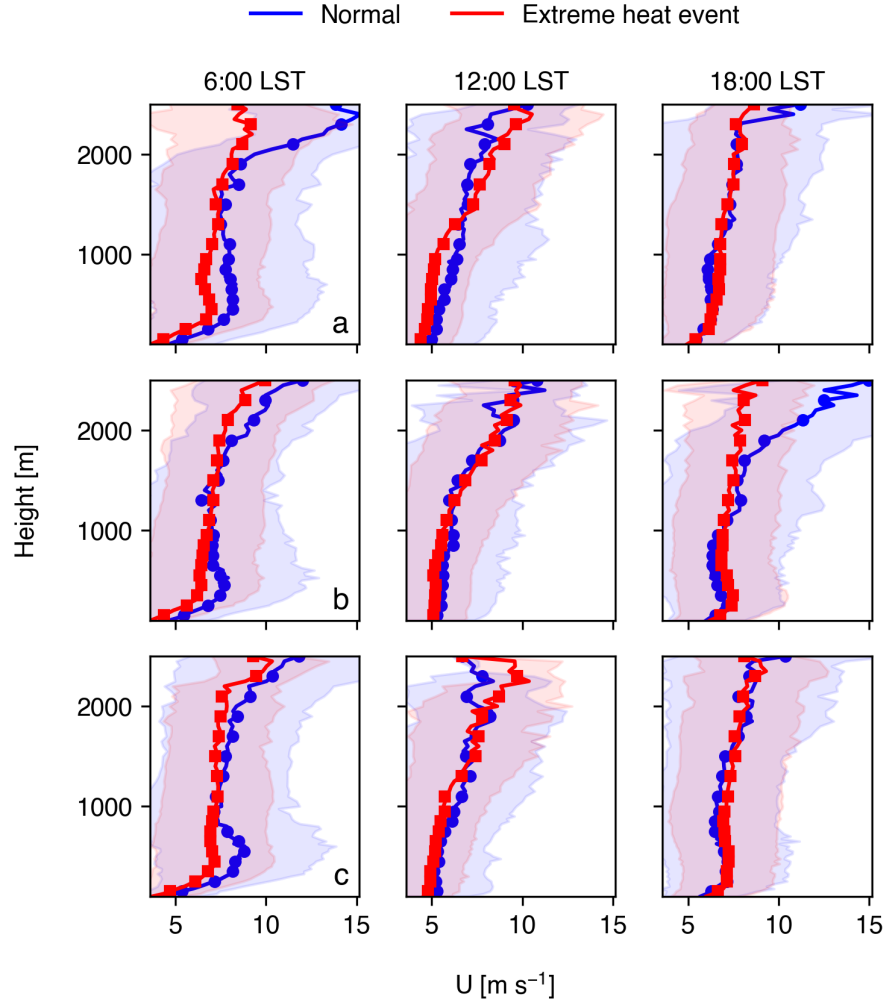


Figure 6: Vertical profiles of  $U$  at the Bronx (a), Queens (b), and Staten Island (c) sites during normal days (blue) and extreme heat events (red).

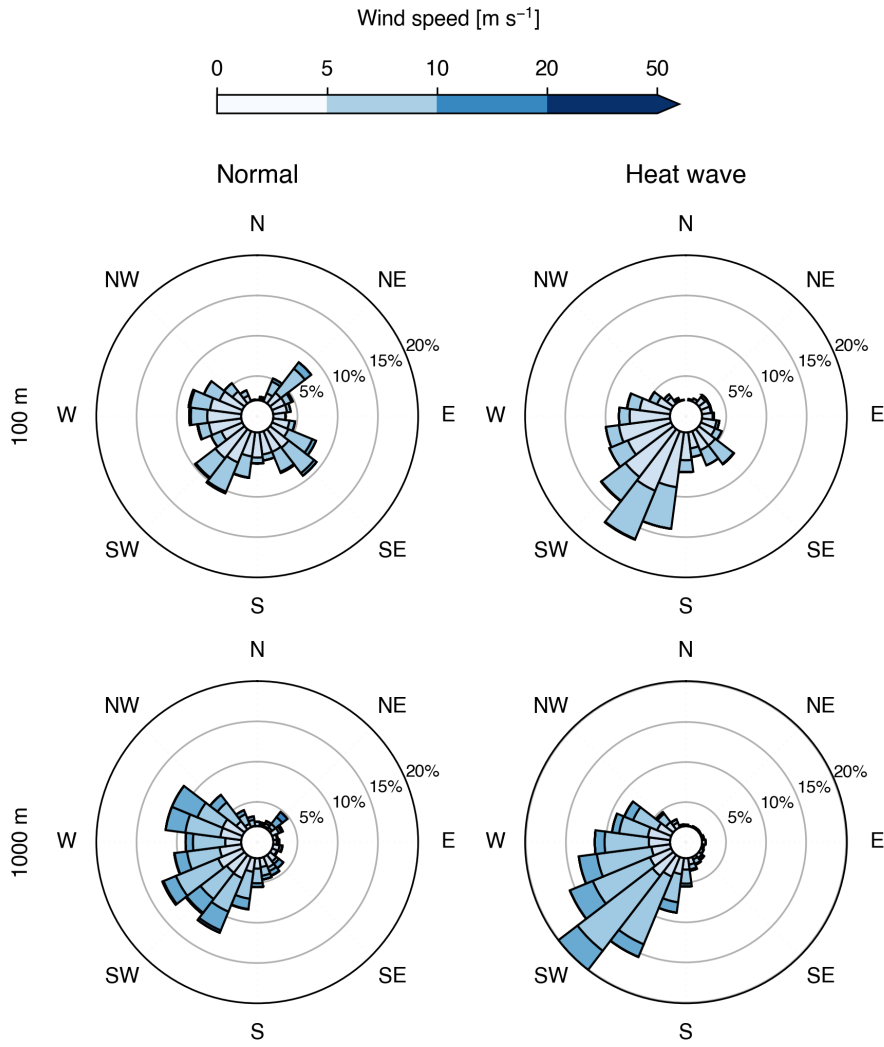


Figure 7: Horizontal winds in the lower-level (100 m) and mid-level of the urban boundary layer over the Bronx.

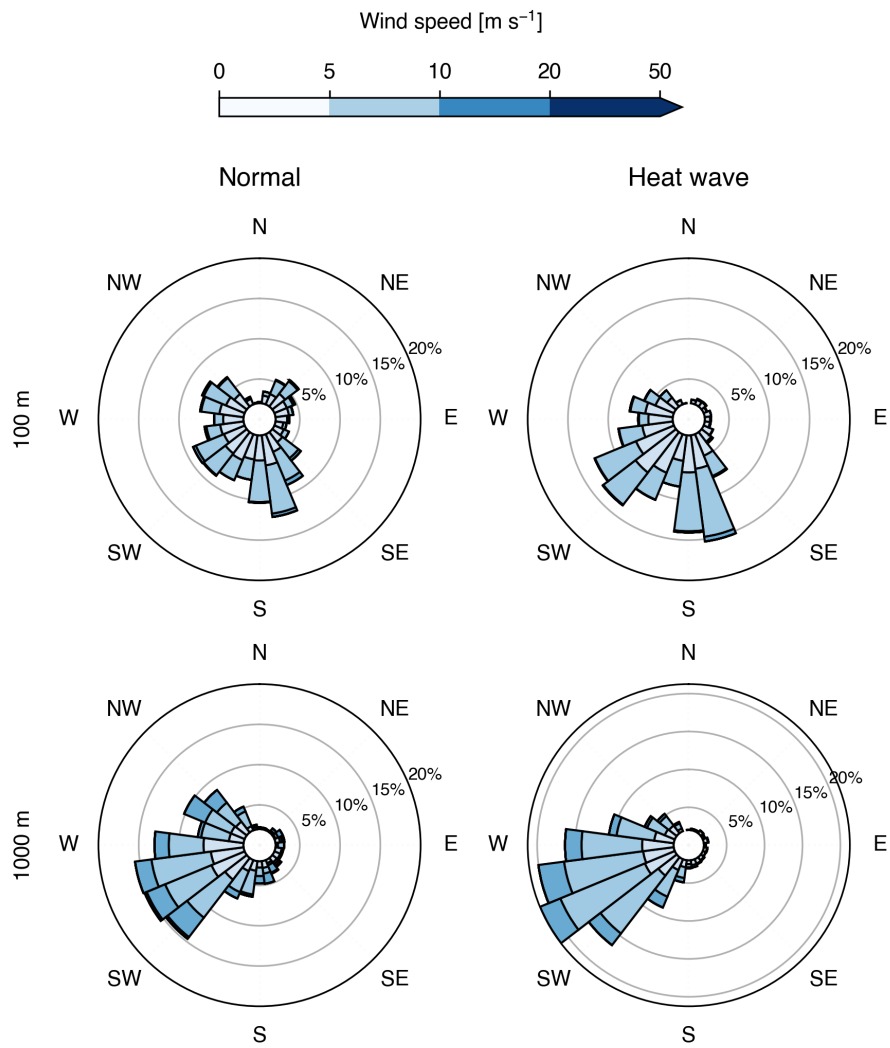


Figure 8: Horizontal winds in the lower-level (100 m) and mid-level of the urban boundary layer over Queens.

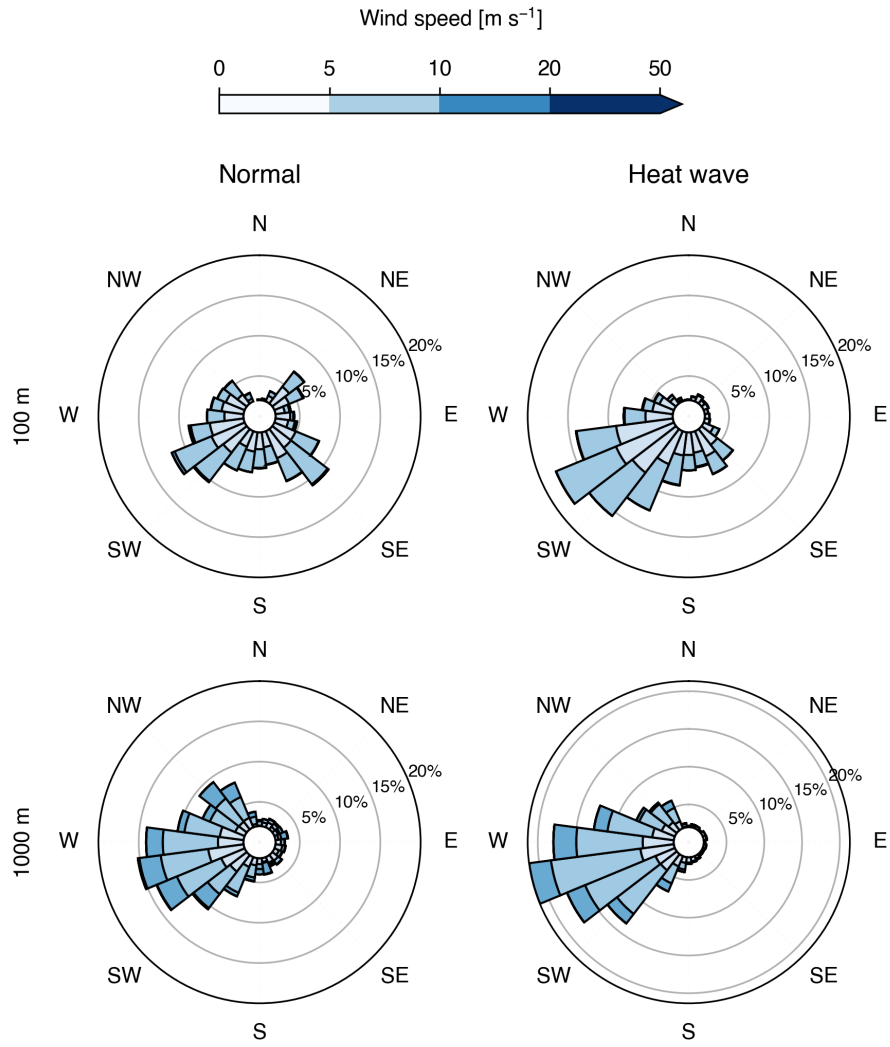


Figure 9: Horizontal winds in the lower-level (100 m) and mid-level of the urban boundary layer over Staten Island.



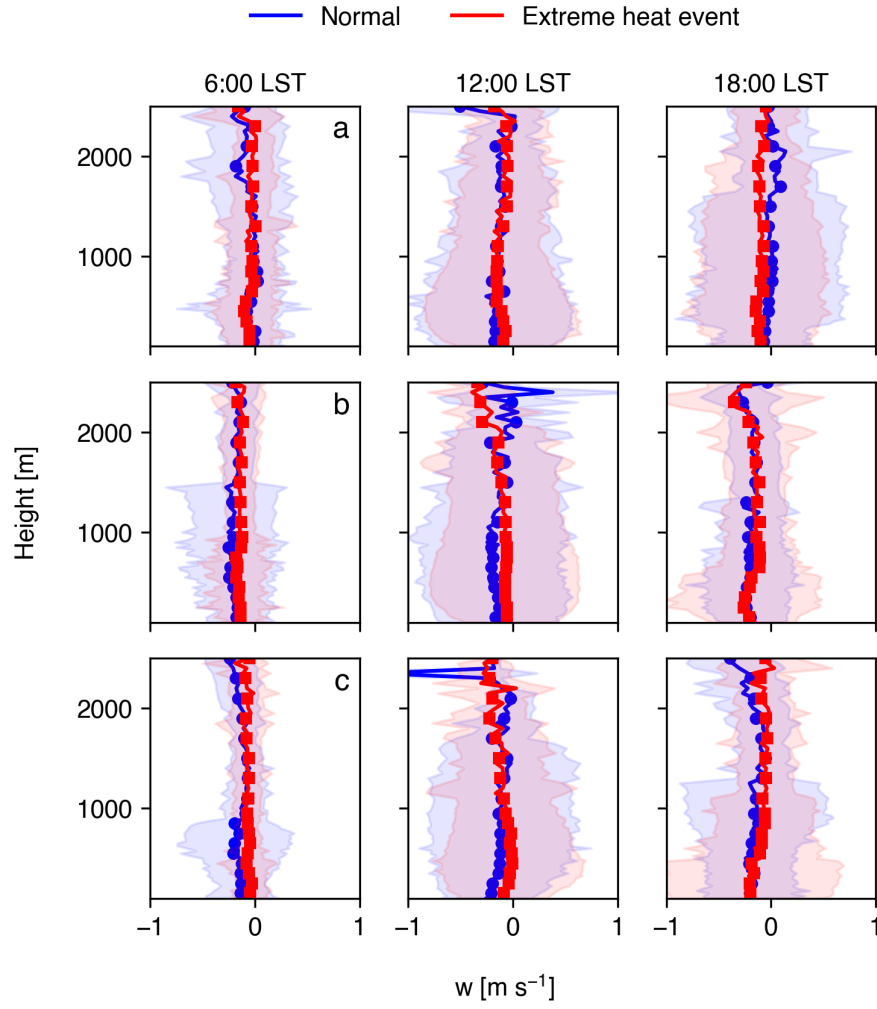


Figure 10: Vertical profiles of  $w$  at the Bronx (a), Queens (b), and Staten Island (c) sites during normal days (blue) and extreme heat events (red).

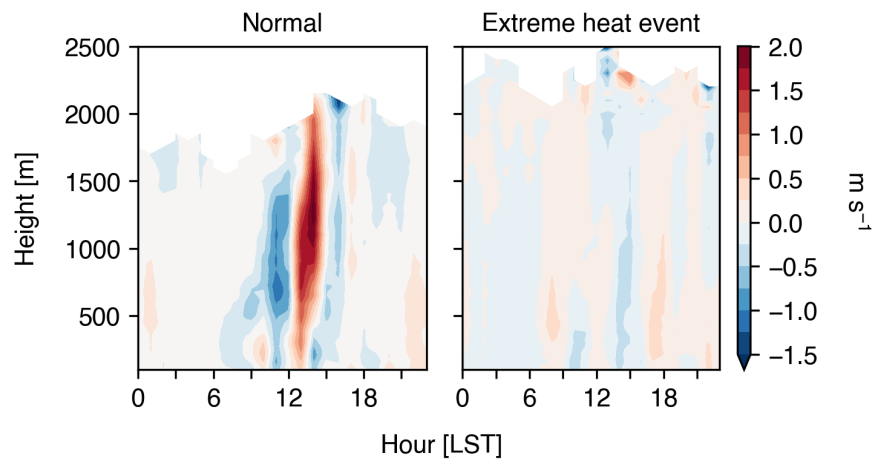


Figure 11: Vertical velocity contours at the Bronx site on a normal (26 July 2019) and extreme heat (29 July 2019) day.

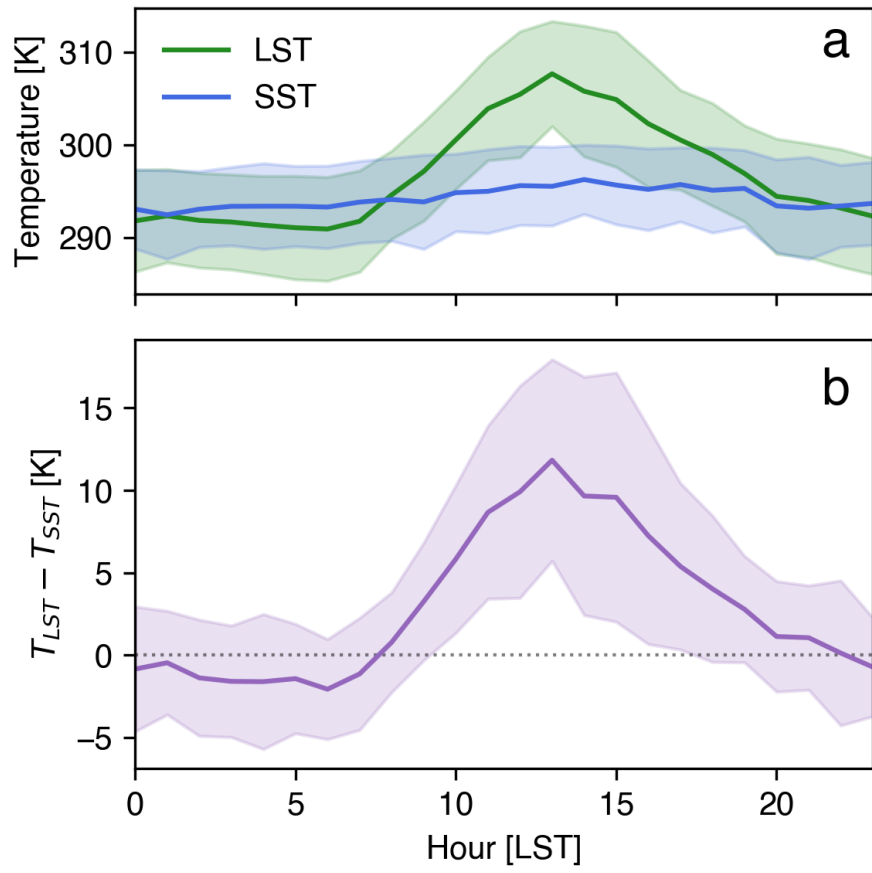


Figure 12: Temperature difference between Queens and New York Bight.

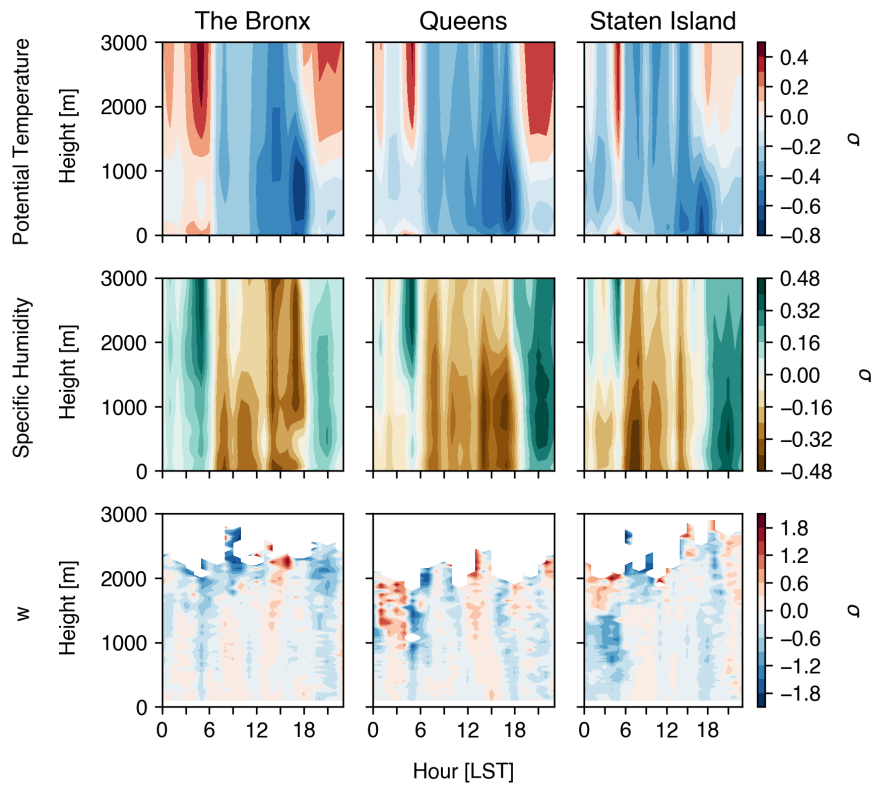


Figure 13: Anomalies for normal days with a sea breeze relative to normal days without a sea breeze.

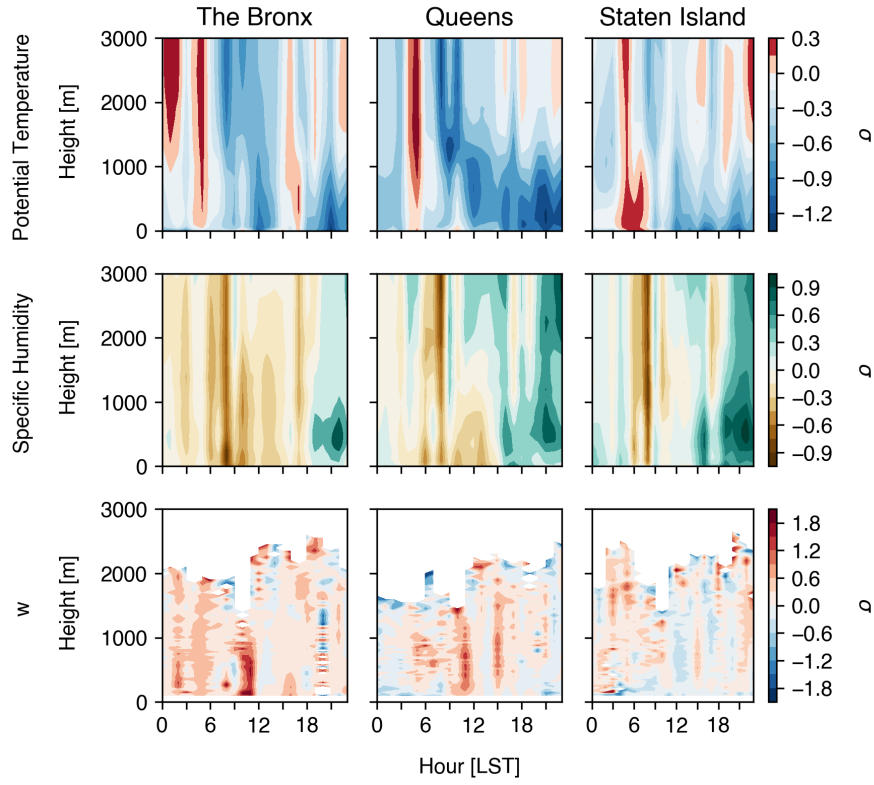


Figure 14: Anomalies for heat wave days with a sea breeze relative to heat wave days without a sea breeze.

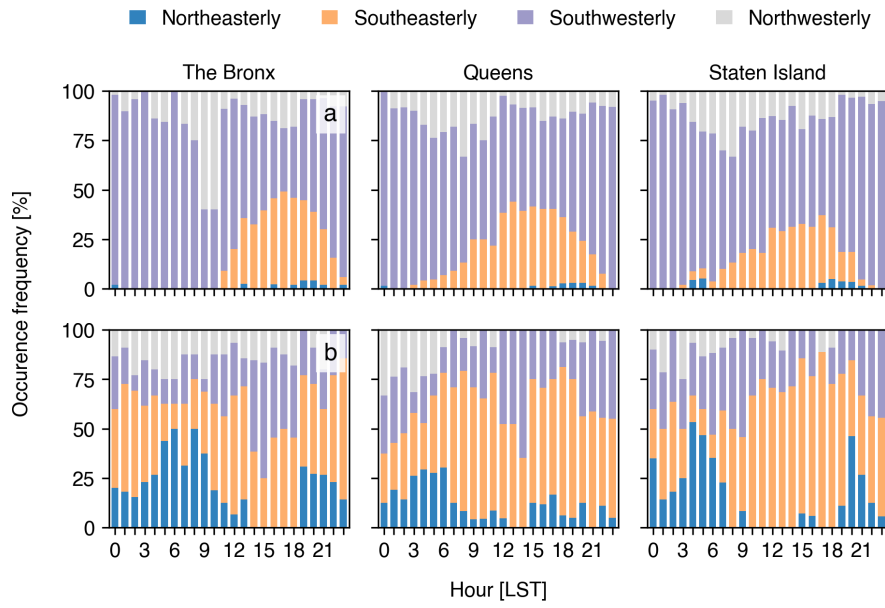


Figure 15: Occurrence frequency of wind directions during (a) extreme heat days without a detected sea breeze and (b) heat wave days with a detected sea breeze, at 100 m at all sites.